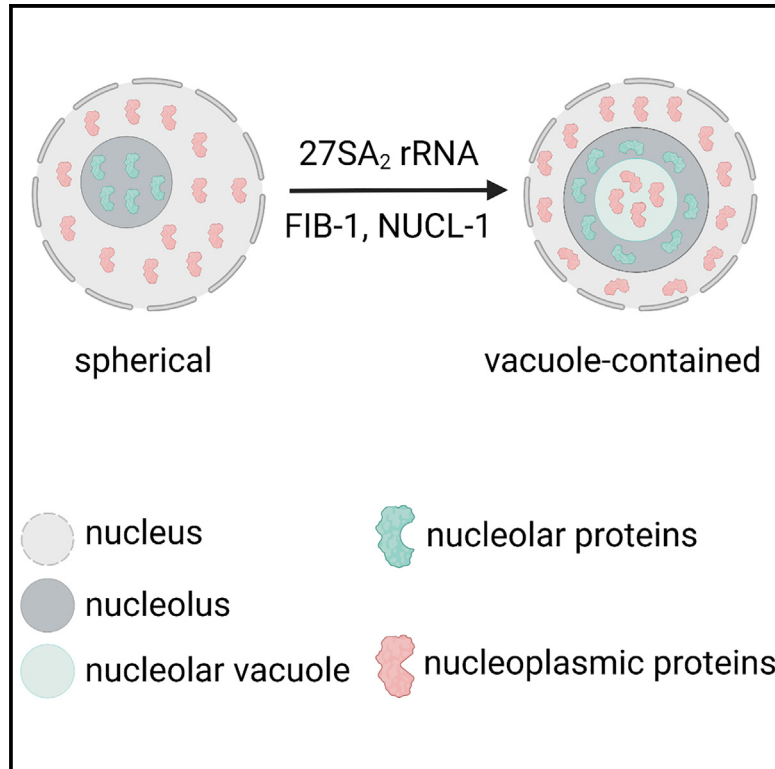


## rRNA intermediates coordinate the formation of nucleolar vacuoles in *C. elegans*

### Graphical abstract



### Authors

Demin Xu, Xiangyang Chen, Yan Kuang, ..., Chengming Zhu, Xuezhu Feng, Shouhong Guang

### Correspondence

zcm916@ustc.edu.cn (C.Z.),  
fengxz@ustc.edu.cn (X.F.),  
sguang@ustc.edu.cn (S.G.)

### In brief

Xu et al. found that the nucleolar vacuole (NoV) contains nucleoplasmic proteins and is capable of exchanging its contents with nucleoplasm. The formation of the NoV is orchestrated by rRNA transcription, processing, and maturation.

### Highlights

- The appearance of nucleolar vacuole is dynamic in *C. elegans*
- Nucleolar vacuoles contain nucleoplasmic proteins
- The accumulation of 27SA<sub>2</sub> rRNAs promotes nucleolar vacuole formation
- FIB-1 and NUCL-1 are required for nucleolar vacuole formation



## Article

# rRNA intermediates coordinate the formation of nucleolar vacuoles in *C. elegans*

Demin Xu,<sup>1,3</sup> Xiangyang Chen,<sup>1,3</sup> Yan Kuang,<sup>1</sup> Minjie Hong,<sup>1</sup> Ting Xu,<sup>1</sup> Ke Wang,<sup>1</sup> Xinya Huang,<sup>1</sup> Chuanhai Fu,<sup>1</sup> Ke Ruan,<sup>1</sup> Chengming Zhu,<sup>1,\*</sup> Xuezhu Feng,<sup>1,\*</sup> and Shouhong Guang<sup>1,2,4,\*</sup>

<sup>1</sup>Department of Obstetrics and Gynecology, The First Affiliated Hospital of USTC, The USTC RNA Institute, Ministry of Education Key Laboratory for Membraneless Organelles & Cellular Dynamics, School of Life Sciences, Division of Life Sciences and Medicine, Biomedical Sciences and Health Laboratory of Anhui Province, University of Science and Technology of China, Hefei, Anhui 230027, China

<sup>2</sup>CAS Center for Excellence in Molecular Cell Science, Chinese Academy of Sciences, Hefei, Anhui 230027, China

<sup>3</sup>These authors contributed equally

<sup>4</sup>Lead contact

\*Correspondence: [zcm916@ustc.edu.cn](mailto:zcm916@ustc.edu.cn) (C.Z.), [fengxz@ustc.edu.cn](mailto:fengxz@ustc.edu.cn) (X.F.), [sguang@ustc.edu.cn](mailto:sguang@ustc.edu.cn) (S.G.)

<https://doi.org/10.1016/j.celrep.2023.112915>

## SUMMARY

The nucleolus is the most prominent membraneless organelle within the nucleus. How the nucleolar structure is regulated is poorly understood. Here, we identified two types of nucleoli in *C. elegans*. Type I nucleoli are spherical and do not have visible nucleolar vacuoles (NoVs), and rRNA transcription and processing factors are evenly distributed throughout the nucleolus. Type II nucleoli contain vacuoles, and rRNA transcription and processing factors exclusively accumulate in the periphery rim. The NoV contains nucleoplasmic proteins and is capable of exchanging contents with the nucleoplasm. The high-order structure of the nucleolus is dynamically regulated in *C. elegans*. Faithful rRNA processing is important to prohibit NoVs. The depletion of 27SA<sub>2</sub> rRNA processing factors resulted in NoV formation. The inhibition of RNA polymerase I (RNAPI) transcription and depletion of two conserved nucleolar factors, nucleolin and fibrillarin, prohibits the formation of NoVs. This finding provides a mechanism to coordinate structure maintenance and gene expression.

## INTRODUCTION

The nucleolus is the most prominent membraneless organelle within the nucleus, which forms around the tandem arrays of ribosomal gene repeats, termed nucleolar organizer regions.<sup>1</sup> The nucleolar proteome identified more than 1,000 different proteins, most of which are involved in ribosome biogenesis, including rRNA transcription and processing and ribosome assembly.<sup>2,3</sup> Increasing works suggest that nucleolus is a multilayered biomolecular condensate and assembles via phase separation.<sup>4–7</sup> *In vitro* reconstitution studies suggested that the key nucleolar proteins, fibrillarin and nucleophosmin, can undergo phase separation.<sup>4</sup> In the *X. laevis* germinal vesicle, nucleoli exhibit liquid-like behavior, spontaneously coalescing and rounding up upon contact.<sup>5</sup> In addition, it was suggested that the organization of nucleolar subcompartments arises through multiphase liquid immiscibility, which is driven by differential surface tension of substructures.<sup>4,8</sup>

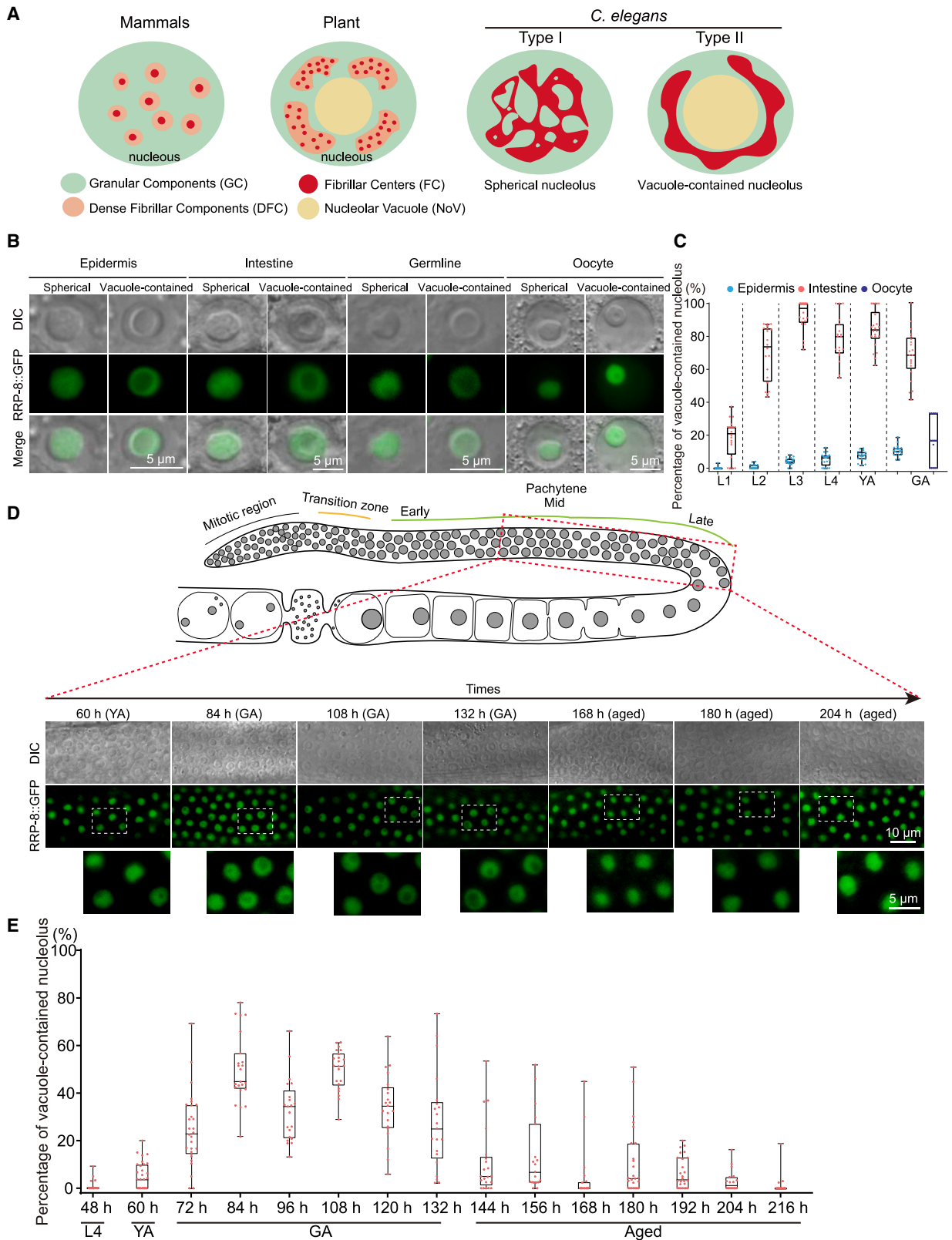
The nucleoli of mammalian cells display three internal phase-separated subcompartments, the fibrillar center (FC), the dense fibrillar component (DFC), and the granular component (GC).<sup>7</sup> Typically, the FC is surrounded by a shell of the DFC; both are enclosed in the GC. Recent work has suggested that *C. elegans* nucleoli also contain two phase-separated subcompartments, the GC and the FC.<sup>9</sup> Besides, there is a highly conserved central region, called the nucleolar cavities or vacu-

oles, present in the nucleoli of various plants and animals, which was firstly observed in the 19<sup>th</sup> century (Figure 1A).<sup>9–13</sup> A similar nucleolar vacuole (NoV) has been observed in mammalian cells, such as in MCF-7, COS-7, and Hep-2 cells.<sup>14</sup>

Although the NoV has been known for more than a hundred years, its regulatory mechanism, composition, and function remain unclear. In *soybean*, different types of cellular stresses and environmental stimuli, for example cold-warm treatment, led to the formation of the NoVs.<sup>15,16</sup> Similarly, the NoV was formed in heat and chilling stress-treated *Arabidopsis thaliana*<sup>17</sup> and 5-fluoro-uracil-treated *Jerusalem artichoke tubers*.<sup>13</sup> Drugs inhibiting rRNA synthesis, including actinomycin D, 5-fluoro-uracil, and 2-thio-uracil, could impede vacuole formation in *tobacco callus* and *zea mays* cells.<sup>18,19</sup> The vacuoles may contain ribonucleoprotein (RNP) complexes because both small nuclear RNAs (snRNAs) and small nucleolar RNAs (snoRNAs) have been detected.<sup>20,21</sup> It was postulated that NoVs may engage in mRNA surveillance and export, transport of nucleolar substance, and temporary storage of certain materials.<sup>12,13,15,22</sup> In addition, bigger vacuoles may link to higher nucleolar activity.<sup>15</sup>

Here, we investigated the nucleolar structure of *C. elegans* and identified two types of nucleoli: spherical and vacuole-contained nucleoli. We conducted candidate-based RNAi screening and identified a distinct class of ribosomal proteins of the large subunit (RPLs), the knockdown of which reshaped spherical nucleoli to vacuole-contained nucleoli and therefore were named class





(legend on next page)

I RPLs. Through a circularized reverse-transcription PCR (cRT-PCR), we detected abnormal accumulation of 27SA<sub>2</sub> rRNAs upon the depletion of class I RPLs. Interestingly, the vacuole-contained nucleoli exhibited reentrant phase-transition behavior by monotonically increasing 27SA<sub>2</sub> pre-rRNAs. We further revealed that nucleoplasmic proteins, rather than rRNA biogenesis-related proteins, usually accumulated in NoVs. NUCL-1 and FIB-1, the two highly conserved nucleolar proteins with internal disordered sequences, were required for the formation of NoVs. Together, this work suggested that the structure of the nucleolus is highly coordinated with rRNA processing and maturation.

## RESULTS

### The appearance of NoVs is dynamic in *C. elegans*

Nucleolar substructure in nematodes is largely unstudied, and the number and composition of subcompartments are mostly unclear. Recent work began to show that *C. elegans* nucleoli also contain two phase-separated subcompartments, the GC and the FC.<sup>9</sup> Interestingly, during the culture of *C. elegans*, we frequently observed the appearance of NoVs by differential interference contrast (DIC) microscopy (Figure S1A). To further explore the nucleolar structure, we generated an RRP-8:GFP transgene to label the nucleoli. RRP-8 is a rRNA processing factor involved in N<sup>1</sup>-methyladenosine (m<sup>1</sup>A) modification of 26S rRNAs.<sup>23,24</sup> The nucleoli were visualized by DIC and fluorescent microscopy, respectively. We identified two types of nucleoli in *C. elegans*. In type I nucleoli that do not have NoVs, RRP-8:GFP likely evenly occupied the entire nucleoli, and the nucleoli were spherical under DIC microscopy (Figure 1B). Therefore, we called them type I spherical nucleoli. Type II nucleoli contain NoVs and revealed altitude differences between the NoV and periphery under DIC microscopy (Figure 1B). RRP-8:GFP was excluded from NoVs and strongly enriched in the periphery of the nucleoli. We named type II nucleoli as vacuole-contained nucleoli, and the nucleolar ring surrounding the NoV likely contains GC and FC subcompartments.<sup>9</sup> The two types of nucleoli can be found in different tissues at distinct developmental stages (Figures 1B and 1C). In epidermal cells and gonadal cells, most nucleoli do not contain NoVs. In contrast, most intestinal nucleoli contain NoVs. The nucleolar structure in the germline is reshaped dynamically during development. In germ cells, the presence of NoVs increased in young gravid adults and reduced in aged animals, suggesting a dynamic regulation of NoVs (Figures 1D and 1E).

### Class I *rpl* genes inhibit NoV formation

The formation of nucleolar subcompartments is tightly linked to ribosome biogenesis.<sup>7</sup> To explore the mechanism and function of NoVs, we conducted a candidate-based RNAi screening to search for factors that are required to maintain the two-shaped nucleoli. We selected 110 genes, including RPLs involved in

60S ribosome assembly as well as 26S rRNA processing, ribosomal proteins of the small subunit (RPSs) involved in 40S ribosome assembly as well as 18S rRNA processing, and other rRNA processing factors, and knocked down these genes by feeding RNAi (Figure 2A; Table S1). Then, we visualized the nucleolar morphology and localization of RRP-8:GFP. From 48 *rpl* genes, knocking down a group of 19 *rpl* genes significantly increased the proportion of vacuole-contained nucleoli (Figures 2B–2D and S1B–S1E). We divided the 48 *rpl* genes into two classes according to whether knocking down the gene could promote the formation of NoVs (Figure 2E). Knocking down class I *rpl* genes significantly increased the size of NoVs (Figures 2F–2H).

The nucleolus is likely formed by phase separation, which could be modulated by environmental temperature.<sup>25</sup> Many disordered proteins and/or nucleic acids, such as FIB1,<sup>25</sup> FUS,<sup>26</sup> Pab1,<sup>27</sup> PGL-3,<sup>28</sup> and homopolymeric RNA,<sup>29,30</sup> undergo phase separation either upon cooling or heating. In addition, heat and chilling stress have been shown to induce the formation of NoVs in *Arabidopsis thaliana*.<sup>17</sup> We investigated the effect of cold stress on NoVs. In wild-type animals, the formation of NoVs was suppressed by 4°C cold stress and reverted when shifting back to 20°C (Figures S2A and S2B). Knocking down class I RPLs, such as *rpl-14*, induced large NoVs in all nucleoli under 20°C. Similarly, the formation of large NoVs upon *rpl-14* RNAi was also strongly prohibited by 4°C cold stress, and the large NoVs reformed after transferring the worms back to 20°C for 24 h (Figures S2C and S2D).

### rRNA transcription and processing machineries are excluded from NoVs

The factors involved in rRNA transcription and processing and ribosome assembly usually localize to the FC, DFC, and GC subnucleolar compartments in mammalian cells.<sup>31</sup> Previous studies showed that the NoV was distinct from the GC, the DFC, and the FC in plants and *C. elegans*.<sup>9,10</sup> To test whether GC-, DFC-, and FC-associated proteins could localize to the NoV, we generated single-copy transgenes of a number of nucleoli-localized proteins by CRISPR-Cas9 technology. Most of the GFP/mCherry tags were inserted at the endogenous genomic loci. All of the transgenes, except the FIB-1:mCherry transgene, could recapitulate the function of the endogenous proteins. The FIB-1:mCherry transgene, although faithfully reflecting the localization of nucleoli, may not recapitulate all functions of FIB-1, which has been shown by our lab and other labs.<sup>32</sup> We examined their localization under wide-field microscopy upon knocking down *rpl-14* by RNAi.

FIB-1 is a conserved fibrillarin involved in nucleogenesis and is usually used as a nucleolar marker.<sup>33,34</sup> RBD-1 is an ortholog of human RBM19, which is required for 90S pre-ribosome maturation.<sup>35</sup> Both FIB-1 and RBD-1 were excluded from large NoVs upon RNAi *rpl-14* (Figures 3A and 3B). RPOA-1, RPOA-2, and RPAC-19 are subunits of the RNA polymerase I complex and were excluded from the large NoVs upon *rpl-14* RNAi (Figures 3C, 3D, and S3A).

### Figure 1. Nucleolar vacuole appearance is dynamic in *C. elegans*

- Schematic diagram of nucleolar structure in mammals, plants, and *C. elegans*.
- Differential interference contrast (DIC) and fluorescent microscopy images of *C. elegans*'s nucleoli in indicated tissues.
- Quantification of the vacuole-contained nucleoli at indicated developmental stages. N > 20 animals.
- DIC and fluorescent microscopy images of the pachytene cells.
- Quantification of the vacuole-contained nucleoli in germline pachytene stage. N > 20 animals.

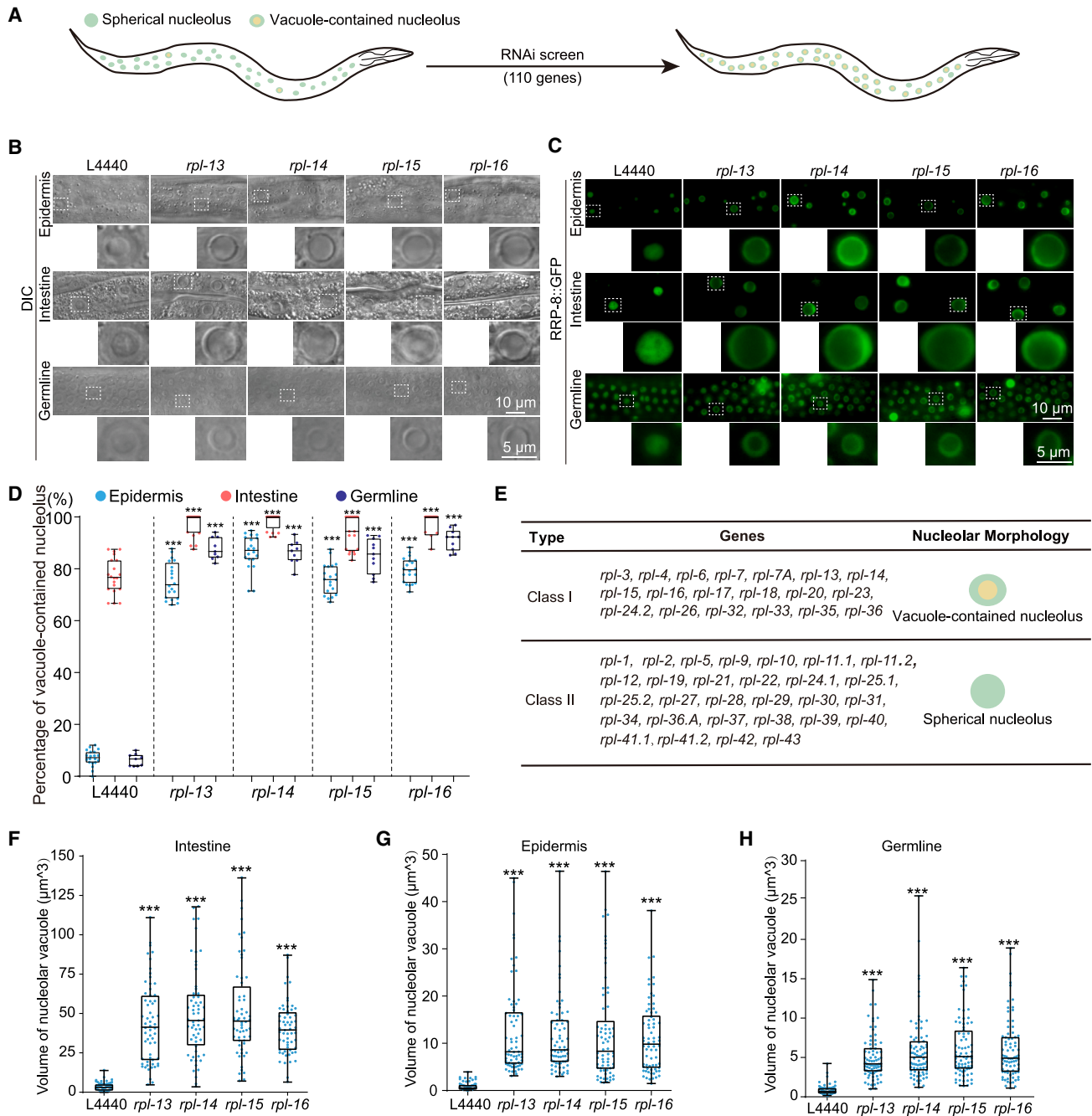


**Figure 2. Class I *rpl* genes limit NoV formation**

(A) Schematic diagram of the candidate RNAi-based genetic screening for the formation of vacuole-contained nucleoli in *C. elegans*'s epidermis.

(B and C) Images of *C. elegans*'s nucleoli after knocking down indicated genes by RNAi in distinct tissues. All worms were imaged at the L3–L4 stage.

(D) Quantification of the vacuole-contained nucleoli after RNAi knocked down indicated genes.  $N > 11$  animals. Significance was tested with two-tailed Student's *t* test. Student's *t* test *p* value threshold was set to 0.05.

(E) Summary of the formation of vacuole-contained nucleoli after knocking down class I and II *rpl* genes.

(F–H) The size of NoVs after RNAi knocked down indicated genes.  $n > 60$  nucleoli from 10 animals. Significance was tested with two-tailed Student's *t* test. Student's *t* test *p* value threshold was set to 0.05.

DAO-5, an rRNA transcription factor, was excluded from the large NoVs upon *rpl-14* RNAi as well (Figure S3B). rRNA processing proteins, for example RPL-7 and T06E6.1, were enriched in the nucle-

olar ring surrounding large NoVs upon *rpl-14* RNAi (Figures S3C and S3D). Additionally, these nucleolar proteins were also excluded from NoVs in wild-type worms as well (Figure S3E).

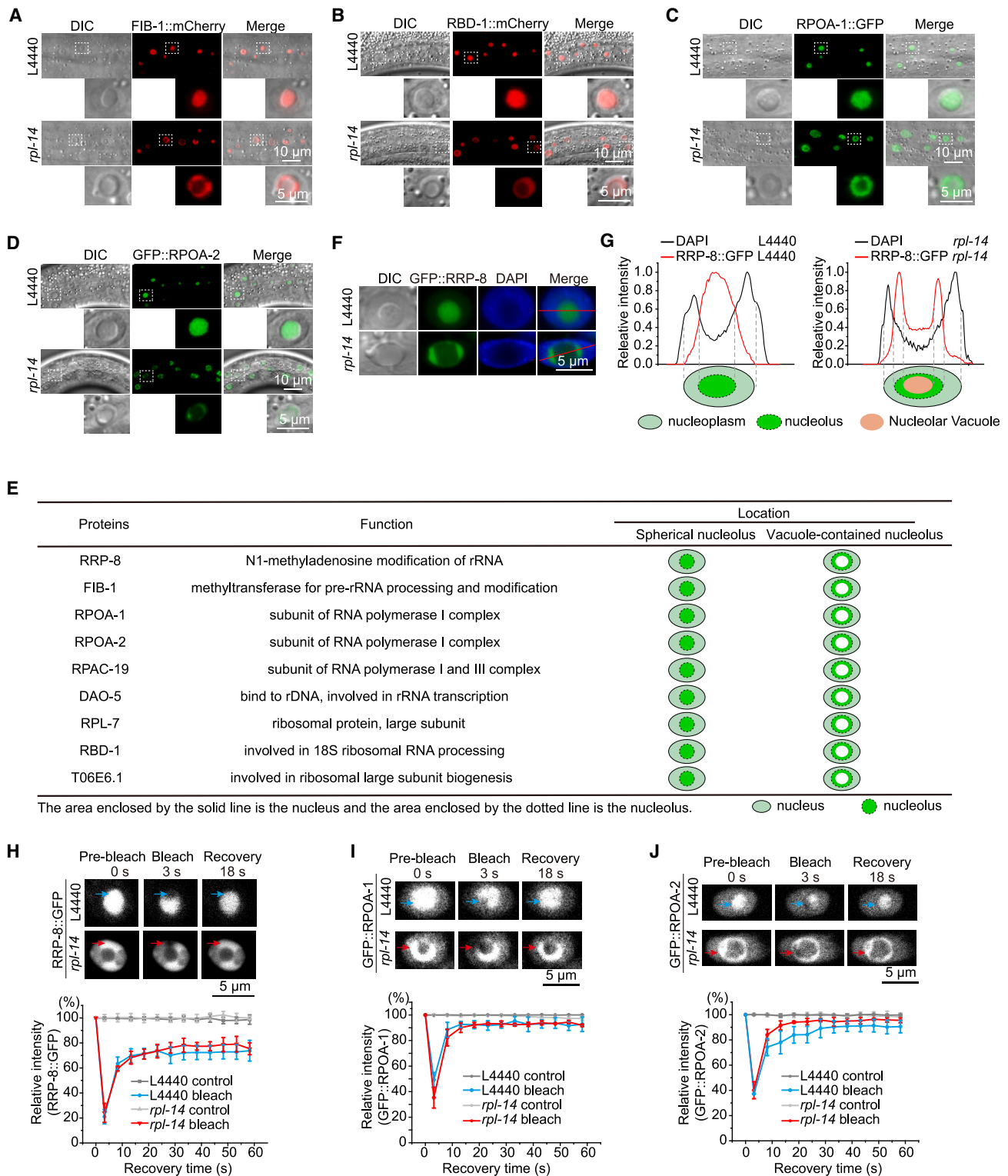


**Figure 3. rRNA transcription and processing factors are excluded from NoVs**  
(A–D) DIC and fluorescent microscopy images of indicated transgenes after knocking down *rpl-14*.  
(E) Summary of the localization of indicated proteins after *rpl-14* RNAi.

(legend continued on next page)

These results are summarized in [Figure 3E](#) and implied that NoVs were different from canonical nucleolar subcompartments and did not contain rRNA transcription and processing factors.

We investigated the localization of nucleic acids in nucleoli. Both DAPI staining and the GFP::HIS-71 (HIS-3.3) transgene indicated that DNA was enriched in the nucleoplasm in both spherical and vacuole-contained nucleoli but was likely depleted from the NoVs ([Figures 3F, 3G, S3F, and S3G](#)). An RNA-specific dye, SYTO RNaselect, was usually used to stain the abundant rRNAs. In control animals, RNA was evenly distributed in the whole spherical nucleoli ([Figures S3H and S3I](#)). Yet, SYTO RNaselect staining was not enriched in NoVs in the vacuole-contained nucleoli, which is consistent with a previous study showing that newly synthesized rRNAs are all localized on the nucleolar ring but not on the NoV in plants.<sup>17</sup> The weak fluorescence in the NoV may be due to the presence of snRNA, snoRNA, or other kinds of RNAs.<sup>21</sup>

The phase-separation ability of nucleoli is essential for its function.<sup>7</sup> We performed a fluorescence recovery after photobleaching (FRAP) assay to investigate whether nucleolar reshaping alters the mobility of rRNA transcription and processing machineries by comparing the mobility of RRP-8, RPOA-1, and RPOA-2 in spherical and vacuole-contained nucleoli. All three proteins did not alter their mobility, respectively, after bleaching ([Figures 3H–3J](#)). These data suggested that nucleolar reshaping may not change the mobility of the components for rRNA transcription and processing and implied that the vacuole-contained nucleoli are still able to conduct the reactions for rRNA transcription, processing, and ribosome assembly.

### Nucleoplasmic proteins are accumulated in NoVs

Previous studies have shown that a number of nucleoplasmic proteins and RNA involved in pre-mRNA processing localized in NoVs, such as spliceosomal protein U2B, U1 snRNA, and the exon-junction complex.<sup>20,36</sup> It was also reported that NoVs revealed nucleoplasmic properties,<sup>37</sup> connected with the nucleoplasm directly in *Sinapis alba*,<sup>38</sup> and transported the content into the nucleoplasm in tobacco BY-2 cells.<sup>10</sup> To investigate the composition of NoVs, we generated a number of fluorescence-labeled transgenes that usually accumulate in the nucleoplasm and are involved in pre-mRNA transcription and processing. We visualized their subcellular localization with and without *rpl-14* RNAi.

AMA-1 is the core subunit of RNA polymerase II. TAF-12 is a subunit of the transcription factor TFIID complex. GTF-2H2C is a subunit of the transcription factor TFIID holo complex. AMA-1, TAF-12, and GTF-2H2C all accumulated in the NoVs in wild-type animals ([Figure S4A](#)) and upon *rpl-14* RNAi ([Figures 4A–4C](#)). MTR-4 and EMB-4 are two pre-mRNA processing factors and are involved in nuclear RNAi.<sup>39,40</sup> NRDE-2 and NRDE-3 are two proteins required for nuclear and nucleolar RNAi.<sup>39,41–43</sup> We observed vacuolar localization of these factors in both wild-type N2 background animals ([Figures S4B and S4C](#)) and *rpl-14* RNAi animals ([Figures S4E–S4H](#)). EXOS-2 is a subunit of the RNA exosome and accumulated in the nucleoplasm, nucleolar ring, and vacuole ([Figure S4D and S4I](#)).

NXF-1 is a mRNA export factor.<sup>44</sup> NXF-1 was highly enriched in the NoVs in wild-type N2 animals and upon *rpl-14* RNAi in epidermal cells ([Figures S5A–S5C](#)). Interestingly, NXF-1 revealed an obvious development-related vacuolar enrichment in germline cells in wild-type animals ([Figures S5D and S5E](#)).

We summarized these data in [Figure 4D](#). Taken together, these data suggested that the NoV contains many mRNA biogenesis and processing factors rather than nucleolar proteins, yet whether there is active mRNA biogenesis and processing in the vacuole is unclear.

The nucleolus is physically separated from nucleoplasm and yet rapidly exchanges its content with the surrounding nucleoplasm.<sup>7</sup> To test whether the nucleolar ring could block the composition exchange between the NoV with the nucleoplasm, we performed a FRAP assay of GFP::NRDE-2 and GFP::MTR-4 in the nucleoplasm and the NoV. Thirty seconds after bleaching, the GFP::NRDE-2 and GFP::MTR-4 fluorescence intensity in the NoV recovered to approximately 60% of the control fluorescent intensity ([Figure 4E](#)). GFP::NRDE-2 exhibited similar mobility by FRAP in the nucleoplasm before and after *rpl-14* RNAi and in the NoV ([Figure 4F](#)). However, GFP::NRDE-2 fluorescence did not recover when the whole nucleus was bleached ([Figure S4J](#)). These data suggested that the proteins inside the NoV could exchange with the components in the nucleoplasm.

### Class I *rpl* genes are required for 27SA<sub>2</sub> rRNA processing

RPLs are proteins of the 60S ribosome subunit that are involved in ribosome assembly as well as pre-rRNA processing.<sup>45</sup> To investigate the mechanism of NoV formation by class I RPL proteins, we adopted a cRT-PCR method to analyze rRNA intermediates upon knocking down *rpl* genes ([Figure 5A](#)).<sup>46,47</sup> We designed primers targeting distinct regions to assay different rRNA intermediates by cRT-PCR ([Figure 5B](#)). To validate the method, we performed cRT-PCR to detect mature rRNA followed by sequencing the ends of mature 5.8S, 18S, and 26S rRNAs ([Figures S6A–S6C](#)). The results were largely consistent with sequences annotated by Wormbase.<sup>48,49</sup>

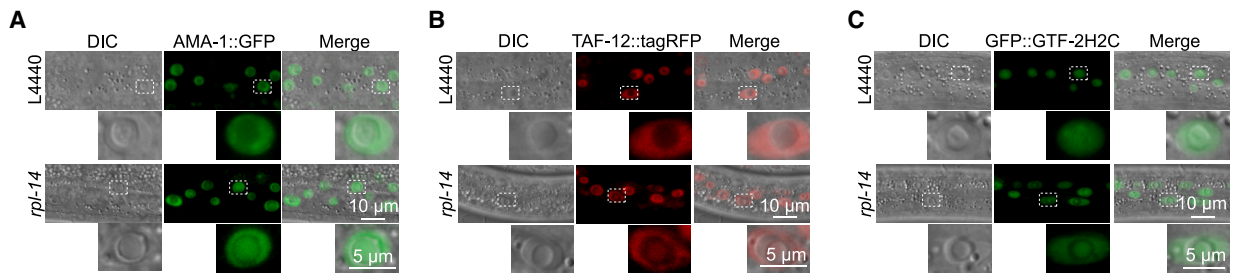
Then, we assayed 26S rRNA intermediates by primer sets partially targeting internal transcribed spacer 2 (ITS2)<sup>50</sup> upon knocking down *rpl* genes ([Figure 5B](#)) and detected two major bands by the cRT-PCR method ([Figure 5B](#)). We cloned and sequenced the 5' and 3' ends of these two bands and confirmed 27SA<sub>2</sub> and 27SB pre-rRNAs ([Figure 5C](#)). Strikingly, knocking down class I *rpl*, but not class II *rpl*, consistently led to the accumulation of 27SA<sub>2</sub> pre-rRNA intermediates ([Figures 5D and 5E](#)), implying that 27SA<sub>2</sub> pre-rRNA or its processing may be involved in the formation of NoVs.

To further confirm that 27SA<sub>2</sub> rRNA is involved in the formation of NoVs, we knocked down 26 predicted 60S rRNA processing factors by RNAi ([Table S1](#)). Feeding RNAi targeting 8 genes led to the formation of NoVs ([Figures S6D and S6E](#)). Most of the eight genes have been reported to be involved in 27SA and 27SB pre-rRNA processing.<sup>51,52</sup> Consistently, 27SA<sub>2</sub> rRNAs were

(F) DAPI staining of epidermal cells after *rpl-14* RNAi.

(G) Fluorescent density scan of GFP::RRP-8 and DAPI staining by ImageJ.

(H–J) (Top) FRAP assay of transgenes in indicated regions before and after *rpl-14* RNAi. (Bottom) Quantification of FRAP data. Mean ± SD, n = 3.



**D**

Proteins	Function	Location	
		Spherical nucleolus	Vacuole-contained nucleolus
NRDE-2	involved in RNA interference and heterochromatin assembly		
NRDE-3	siRNA binding activity. Involved in RNA import into nucleus		
MTR-4	involved in RNA catabolic process and maturation of 5.8S rRNA		
EMB-4	involved in pre-mRNA processing		
AMA-1	involved in mRNA transcription by RNA polymerase II		
TAF-12	subunit of transcription factor TFIID complex		
GTF-2H2C	subunit of transcription factor TFIIF holo complex		
HIS-71	ortholog of human H3-3B		
NXF-1	involved in mRNA export from nucleus		
EXOS-2	subunit of RNA exosome		

The area enclosed by the solid line is the nucleus and the area enclosed by the dotted line is the nucleolus. nucleus nucleolus

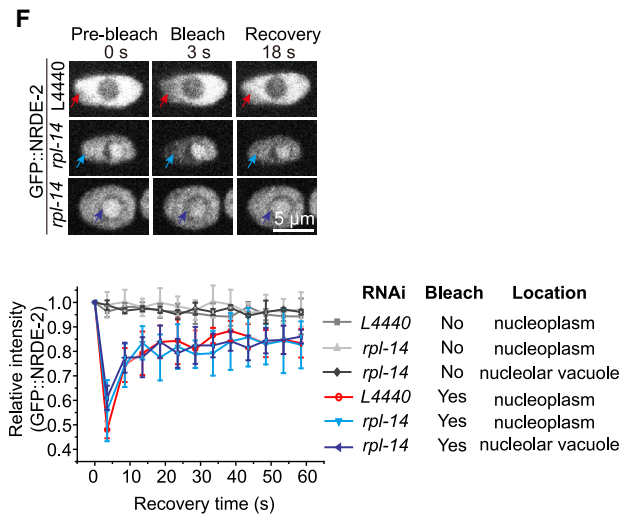
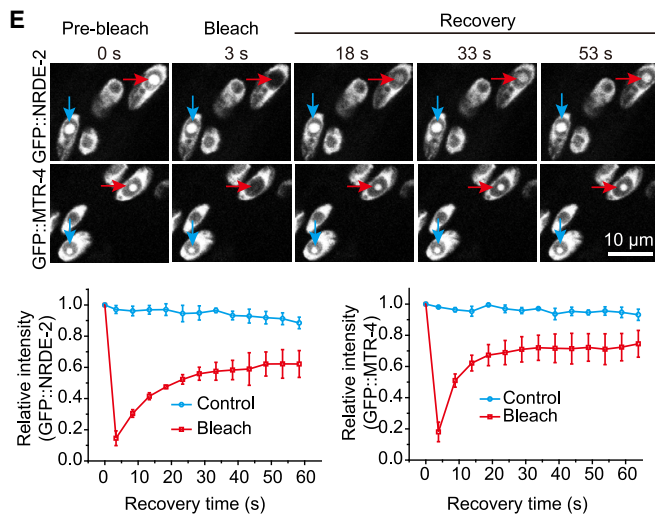


**Figure 4. The NoV contains nucleoplasmic proteins**

(A–C) DIC and fluorescent microscopy images of indicated transgenes after knocking down *rpl-14*.

(D) Summary of the localization of indicated proteins after *rpl-14* RNAi.

(E and F) (Top) FRAP assay of GFP::NRDE-2 and GFP::MTR-4 in indicated regions. (Bottom) Quantification of FRAP data. Mean ± SD, n = 3.

accumulated upon knocking down these genes, as assayed by cRT-PCR (Figures S6F and S6G).

Taken together, these data suggested that rRNA processing steps or intermediates were involved in the maintenance of the nucleolar structure.

**FIB-1 and NUCL-1 are required for NoV formation**

The intrinsically disordered region (IDR) is likely one of the driving forces of phase separation and has been identified in many phase-separated proteins.<sup>4,5,3,5,4</sup> In addition, the GAR/RGG domain is an RNA-binding segment that frequently presents in

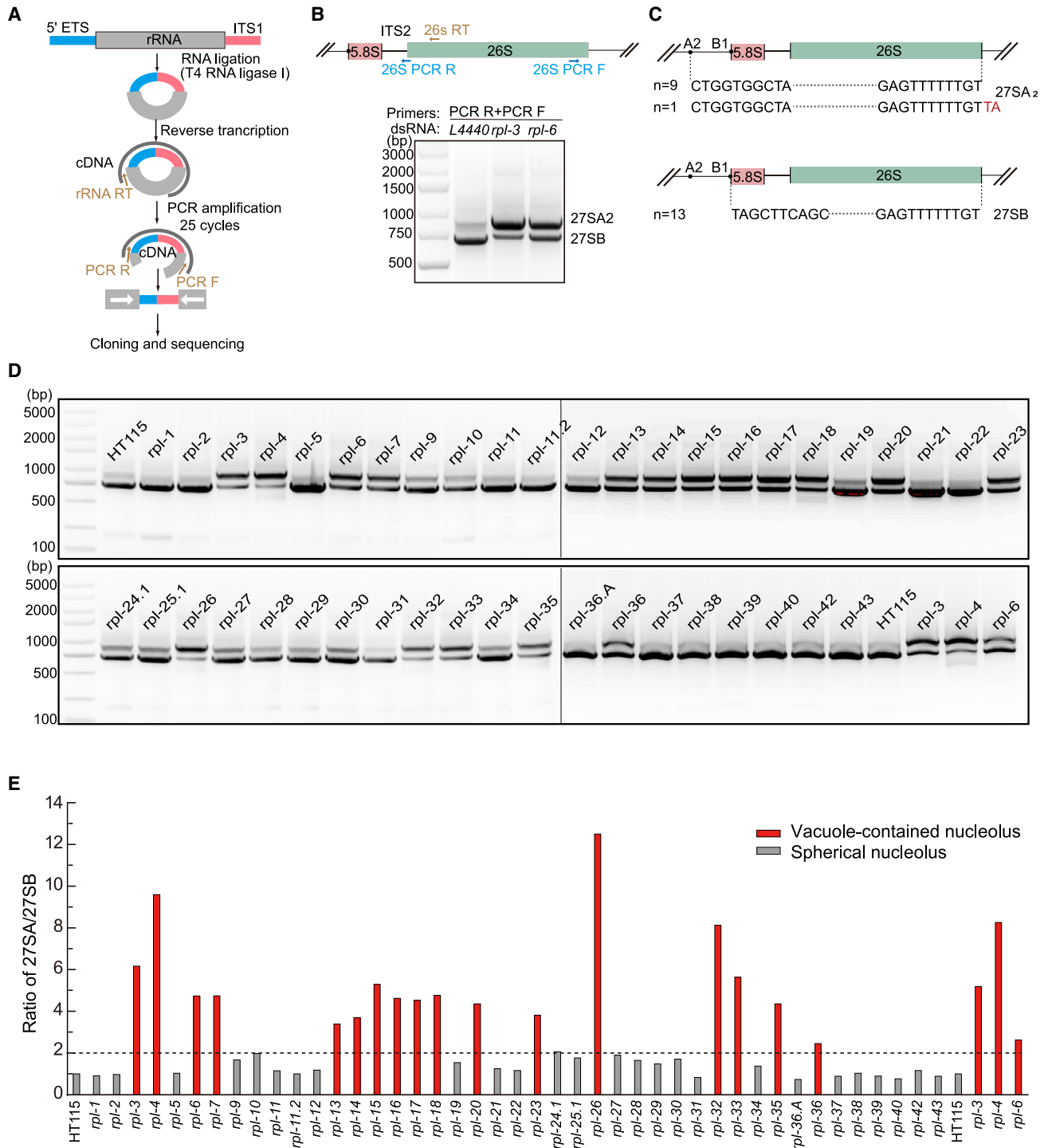


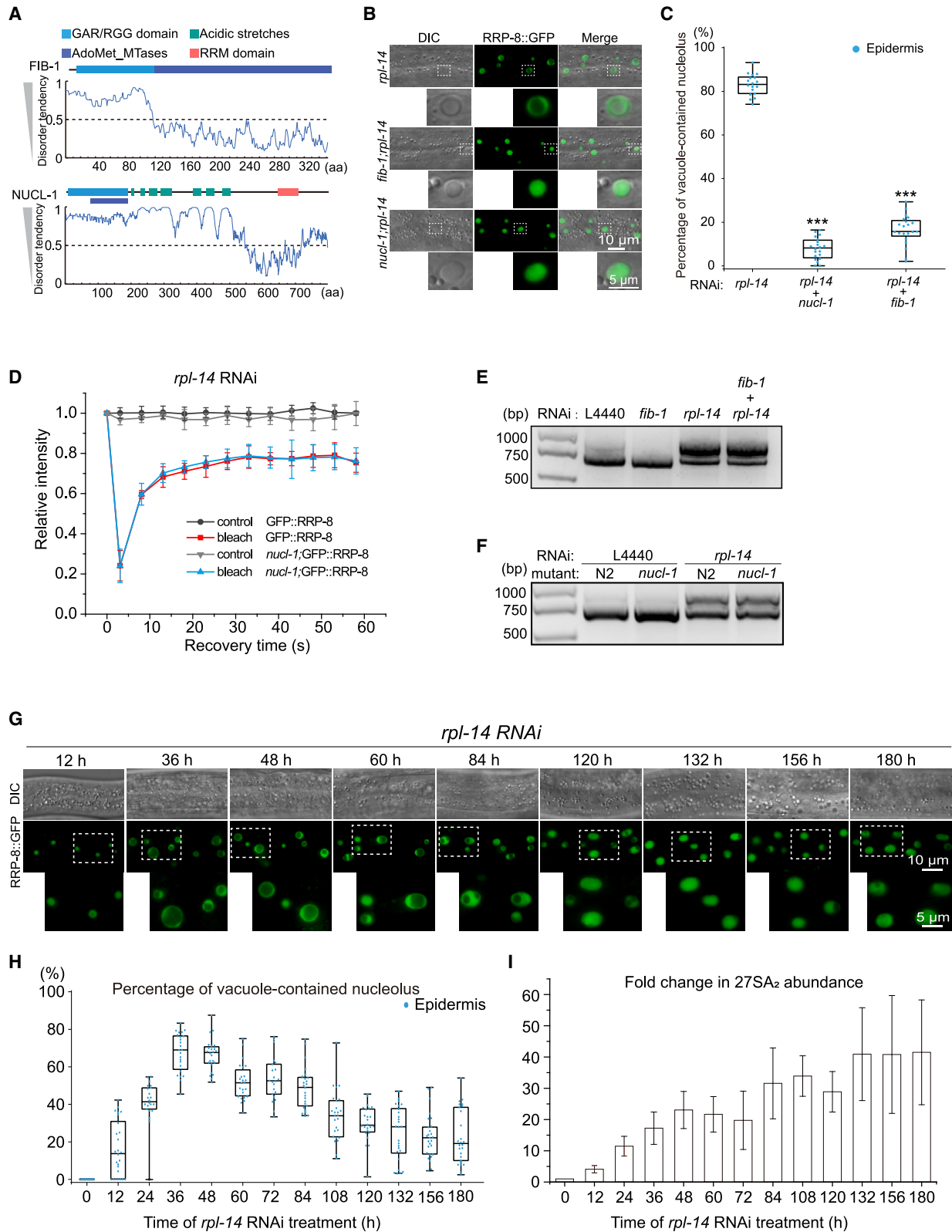
**Figure 5. Class I *rpl* genes are required for 27SA<sub>2</sub> rRNA processing**

(A) Schematic diagram of circularized reverse-transcription PCR (cRT-PCR) method.

(B) cRT-PCR assay of 26S pre-rRNA intermediates.

(C) Sanger sequencing of the ends of 27SA<sub>2</sub> and 27SB rRNAs. n represents the number of clones sequenced.

(D and E) cRT-PCR assay (D) and quantification (E) of 27SA<sub>2</sub> and 27SB pre-rRNA intermediates after knocking down indicated *rpl* genes by RNAi.



(legend on next page)

proteins capable of conducting phase separation.<sup>53–55</sup> To further understand the mechanism of NoV formation, we searched *C. elegans*'s genome for proteins that have both IDR and GAR/RGG domains and that are predicted to localize in the nucleoli. We identified 8 proteins (Figures 6A and S7A), among which knocking down *nucl-1* and *fib-1* strongly blocked the formation of knockdown *rpl-14*-induced vacuole-contained nucleoli (Figures 6B and 6C).

FIB-1 is a highly conserved nucleolar protein with the GAR/RGG domain and the methyltransferase domain that is involved in the methylation of pre-rRNAs and nucleogenesis by phase separation.<sup>4,22</sup> NUCL-1 encodes an evolutionarily conserved protein exhibiting extensive homology to yeast and human nucleolin.<sup>9</sup> The N-terminal domain of NUCL-1 is a long IDR containing a GAR/RGG domain, a methyltransferase domain, and acidic stretches (Figure 6A). The C terminus of NUCL-1 harbors an RRM domain. Previous studies showed that nucleolin associates with nascent pre-rRNA.<sup>56</sup> Nucleolin in mammalian cells displays high mobility and is likely involved in phase separation.<sup>57</sup> To confirm that NUCL-1 is required for the formation of NoVs, we generated two additional deletion alleles of *nucl-1* by CRISPR-Cas9 technology (Figure S7B). Both alleles inhibited the formation of knockdown *rpl-14*-induced vacuole-contained nucleoli (Figures S7C and S7D). The FRAP assay revealed that the spherical nucleoli exhibited similar mobility in *nucl-1; rpl-14* animals to those in control animals (Figure 6D). cRT-PCR showed that FIB-1 and NUCL-1 did not block the accumulation of 27SA<sub>2</sub> rRNA (Figures 6E, 6F, S7E, and S7F), which suggested that FIB-1 and NUCL-1 functioned downstream of 27SA<sub>2</sub> rRNA accumulation.

*In vitro* experiments showed that monotonically increasing RNA concentration could induce the formation of dynamic hollow condensates at high RNA-to-RNP ratios, but a disappearance at further higher RNA-to-RNP ratios, through multivalent heterotypic interactions that mediate a reentrant phase transition of RNPs containing an arginine-rich IDR.<sup>58–60</sup> To test whether nucleoli show a similar behavior *in vivo* during the nucleolar reshaping process, we conducted a time course of *rpl-14* RNAi and examined the nucleolar morphology. Surprisingly, knocking down *rpl-14* induced the formation of NoVs during the early phase of RNAi, yet the NoVs gradually disappeared after long-term *rpl-14* RNAi (Figures 6G and 6H). Consistently, 27SA<sub>2</sub> rRNA monotonically increased during the time course of *rpl-14* RNAi (Figures 6I and S7G).

Taken together, we speculated that NUCL-1 and FIB-1 participate in the regulation of NoVs through phase transition.

### Actinomycin D treatment prohibits NoV formation

Nucleoli undergo dramatic changes when encountering cellular stresses and environmental stimuli. Previous studies revealed that actinomycin D, which inhibits RNA polymerase I activity, could impede vacuole formation.<sup>18,19</sup>

To investigate the reshaping mechanism of spherical nucleoli to vacuole-contained nucleoli, we knocked down *rpl-14* by RNAi in the presence of actinomycin D. A 10 μg/mL actinomycin D treatment did not noticeably change the localization of RRP-8 and the size of nucleoli in wild-type N2 animals (Figure 7A), but it did inhibit the formation of knockdown *rpl-14*-induced NoVs (Figures 7B and 7C). At a higher concentration of actinomycin D (20 μg/mL), the *rpl-14*-induced NoVs were completely inhibited, and RRP-8 likely accumulated as a nucleolar cap structure.<sup>61</sup> Consistently, actinomycin D treatment inhibited the accumulation of knockdown *rpl-14*-induced 27SA<sub>2</sub> rRNA intermediates by cRT-PCR assay (Figure 7D).

### DISCUSSION

The nucleolus is the most important membraneless organelle in the cell. Here, we observed two types of nucleoli, spherical and vacuole-contained nucleoli. The knocked down class I RPL proteins, which are involved in 27SA<sub>2</sub> rRNA processing, induced NoV formation and reshaped the spherical nucleoli to vacuole-contained nucleoli (Figure 7E). In the vacuole-contained nucleoli, rRNA transcription and processing factors accumulated in the nucleolar ring, and a large number of nucleoplasmic proteins accumulated in the NoV. The inhibition of RNA polymerase I (RNAPI) transcription by actinomycin D and the depletion of two conserved nucleolar factors, nucleolin and fibrillarin, prohibit the formation of NoVs.

### The nucleolar subcompartments in *C. elegans*

Nucleolar morphology and subcompartments have been studied extensively in mammalian cells. However, the substructure and regulatory mechanism of *C. elegans*'s nucleoli are mysterious. The RG/RGG domains of FIB-1 and NUCL-1 are required for subnucleolar compartmentalization.<sup>9</sup> Here, we observed that the vacuole-contained nucleoli all contained a large NoV upon knocking down class I RPLs. We divided the vacuole-contained nucleoli into two parts: the NoV and a nucleolar ring surrounding the NoV. We did not exactly know whether the appearance of the NoV induced the formation of the nucleolar ring or whether the formation of the nucleolar ring triggered the appearance of a vacuole inside. Since the NoV contains nucleoplasmic proteins and the ring is the region of the GC and FC subcompartments, which

### Figure 6. FIB-1 and NUCL-1 are required for NoV formation

- (A) Schematic diagram of domain structure and predicted intrinsically disordered regions of NUCL-1 and FIB-1.  
 (B) DIC and fluorescent microscopy images of indicated epidermal cells upon RNAi targeting indicated genes.  
 (C) Quantification of vacuole-contained nucleoli in epidermal cells. N = 20 animals. Significance was tested with two-tailed Student's t test. Student's t test p value threshold was set to 0.05.  
 (D) FRAP assay of GFP::RRP-8 in *nucl-1* mutants. Mean ± SD, n = 3.  
 (E) cRT-PCR assay of 27SA<sub>2</sub> and 27SB pre-rRNA intermediates after knocking down indicated genes by RNAi.  
 (F) cRT-PCR assay of 27SA<sub>2</sub> and 27SB pre-rRNA intermediates of *nucl-1* mutant after knocking down *rpl-14* by RNAi.  
 (G) DIC and fluorescent microscopy images of indicated epidermal cells upon *rpl-14* RNAi over time.  
 (H) Quantification of vacuole-contained nucleoli in epidermal cells. N = 20 animals.  
 (I) Expression levels of 27SA<sub>2</sub> pre-rRNAs quantified by real-time PCR. Mean ± SD, n = 3.

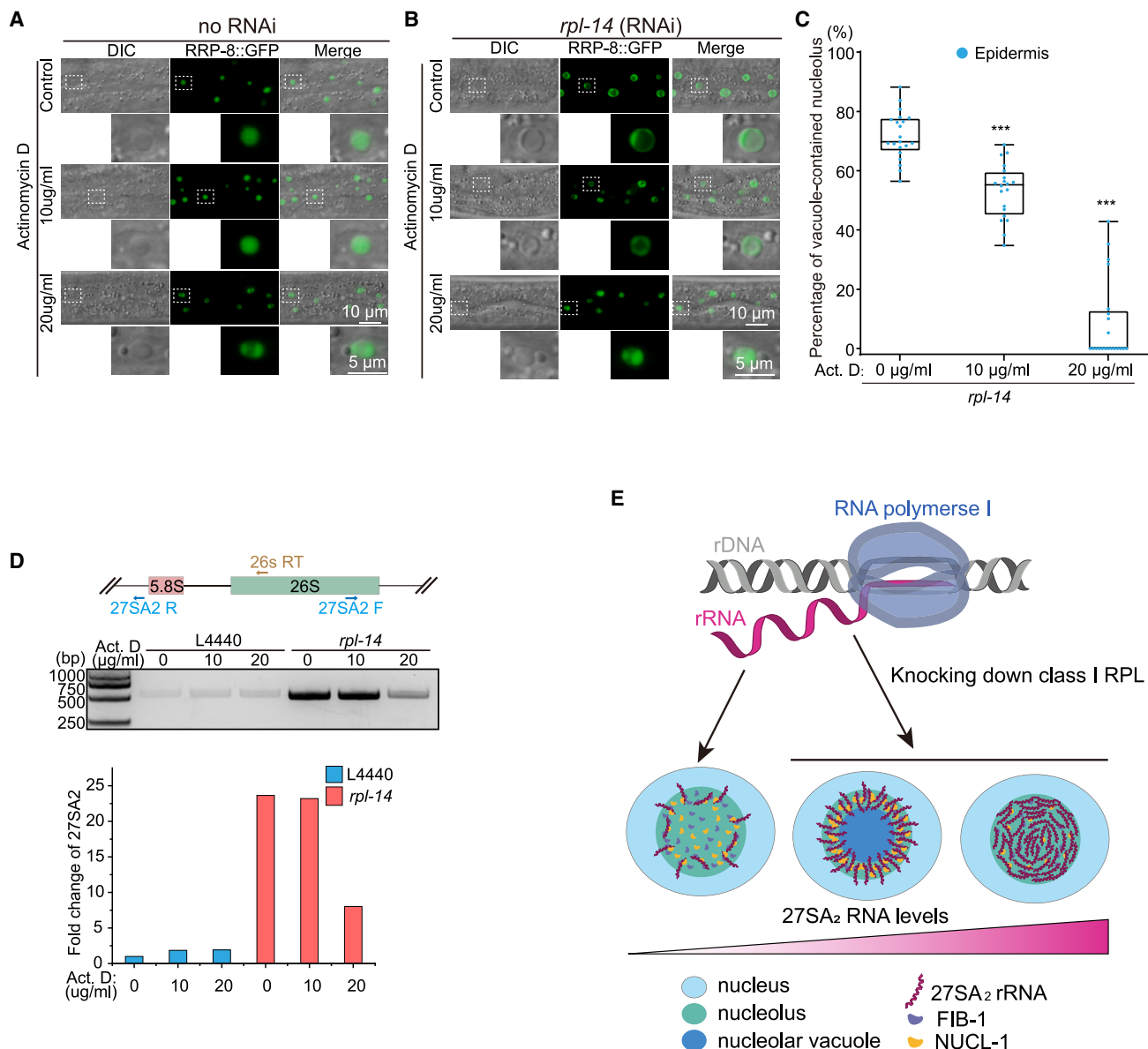


**Figure 7. rRNA transcription and maturation are required for NoV formation**

(A and B) DIC and fluorescent microscopy images of indicated epidermal cells after actinomycin D (Act. D) treatment, without (A) or with (B) *rpl-14* RNAi. (C) Quantification of vacuole-contained nucleoli after Act. D treatment in the presence of *rpl-14* RNAi. N = 20. Significance was tested with two-tailed Student's t test. Student's t test p value threshold was set to 0.05. (D) (Top) cRT-PCR assay and (bottom) quantification of 27SA<sub>2</sub> pre-rRNA intermediates after Act. D treatment in the presence of *rpl-14* RNAi. (E) A working model of rRNA intermediate-directed nucleolar reshaping.

contain proteins required for rRNA processing, together with the fact that 27SA<sub>2</sub> rRNA processing factors and two nucleolar proteins are involved in the formation of the NoV, we speculated that it is very likely that the formation of a nucleolar ring will induce the appearance of a NoV inside the ring.

#### Regulation of nucleolar morphology by 27SA<sub>2</sub> rRNA

The formation of multiphasic nucleolar structure may be due to the interaction of nucleolar proteins and rRNAs.<sup>4</sup> Here, we found that the factors inhibiting the formation of vacuole-contained

nucleolus are all involved in 27SA<sub>2</sub> rRNA processing, suggesting that the 27SA<sub>2</sub> rRNA intermediates may play an important role in nucleolar morphology regulation. Similar to the vacuole-contained nucleolus, [RGRGG]<sub>5</sub> polypeptides and cellular RNAs can form hollow condensates *in vitro*.<sup>60</sup> An *in vitro* experiment indicated that monotonically increasing the RNA concentration in mixtures of synthetic peptides containing multivalent arginine-rich linear motifs can induce dynamic droplet substructure formation and disappearance.<sup>58</sup> A poly-L-lysine and single-stranded oligodeoxynucleotide droplet was shown to undergo

repeated cycles of vacuole nucleation, growth, and expulsion in applied electric fields.<sup>62</sup> The RNA-binding protein TDP-43 can also form hollow condensates in cells by phase separation, if its RNA-binding capacity was disrupted.<sup>63</sup> Here, we found that in *C. elegans*, the nucleoli exhibited similar phase-transition behavior upon *rpl-14* RNAi, which can be inhibited by knocking down two conserved RNA-binding proteins, NUCL-1 and FIB-1, both of which contain an arginine-rich IDR. Further experiments are required to test the causative relation between 27SA<sub>2</sub> rRNAs and the formation of NUCL-1 or FIB-1 hollow condensates. Additionally, rRNA processing and maturation steps are highly conserved among eukaryotes. It will be very interesting to test whether 27SA<sub>2</sub> rRNAs are involved in the maintenance of the hollow structure in plants or the DFC/GC regions in mammalian cells.

It is unclear how and why 27SA<sub>2</sub> rRNAs are involved in the formation and disappearance of vacuole-contained nucleoli. We failed to observe nucleolar reshaping by injecting *in-vitro*-transcribed 27SA<sub>2</sub> rRNAs into *C. elegans*'s germline. It is unclear whether the *in-vitro*-transcribed rRNAs could diffuse into the nucleus or whether they require certain nucleotide modifications. Previous work showed that N<sup>6</sup>-methyladenosine (m<sup>6</sup>A) modification of mRNAs can also induce m<sup>6</sup>A-binding proteins to undergo phase separation.<sup>64</sup> Further investigations are required to investigate the role of 27SA<sub>2</sub> rRNA in driving nucleolar reshaping in *C. elegans*.

### Phase transition of a multilayered nucleolar condensate

According to the reentrant phase-transition model, the condensation is driven by electrostatic attraction between the negatively charged RNAs and the positively charged R/G-rich IDR polypeptide.<sup>58</sup> RNA has a stoichiometry-dependent effect on the phase transition of proteins.<sup>60</sup> At low RNA levels, the electrostatic interactions between RNA and protein induce the formation of condensates, where the condensate surfaces are decorated with the bare segments of RNA chains. The condensates are stabilized due to the low interfacial energy. Yet, excess negatively charged RNAs lead to the accumulation of a large number of counterions on the surface of the positively charged condensates, which increases the total free energy of the system and triggers a long-range electrostatic repulsion to prevent protein condensation.<sup>58,60</sup> The formation of hollow condensation provides an additional interface allowing redistribution of bare RNA chains within the vacuole, thereby reducing the free energy of the system.<sup>60</sup> In addition, an interplay between short-range cation- $\pi$  attraction and long-range electrostatic repulsion may tune reentrant phase transition.<sup>59</sup> The charge balance of electrostatic interactions may be crucial for retaining transcriptional condensate *in vivo*.<sup>65</sup> Based on these studies, we speculated that knocking down class I RPLs may accumulate 27SA<sub>2</sub> rRNAs and invert charges of nucleolar RNPs, resulting in nucleolar reshaping.

Alternatively, nucleolar subcompartments may be formed by distinct protein droplets with different surface tensions.<sup>4,8</sup> For instance, HSP70 family proteins are enriched in the central of hollow condensation and retain the morphology of TDP43 spherical shells.<sup>63</sup> The NoV of *C. elegans* was enriched with many nucleoplasmic proteins. Whether these nucleoplasmic proteins

are involved in nucleolar reshaping is unclear. It will be very interesting to test whether the morphology of the vacuole-contained nucleoli is maintained by certain specific proteins in the NoV or by some disorder proteins on the nucleolar ring.

Previous reports showed that the inhibition of nucleolar function can dramatically alter its structure.<sup>61,66</sup> Here, the inhibition of RNAPI by actinomycin D prohibited the formation of the vacuole-contained nucleoli, yet the mechanism is unclear. *C. elegans* exhibits different proportions of vacuole-contained nucleoli in distinct tissues. Whether and how development and environmental stimuli reshape nucleolar structure require further investigation.

It is unclear how and why cold stress induced nucleolar reshaping. Previous reports showed that integrated stress responses specifically inhibit the first step of rRNA processing when cells encounter stress and that unprocessed rRNAs are stored within the nucleolus and maintain nucleolar integrity.<sup>67</sup> When the stress is resolved, rRNAs reenter the processing and maturation pathway. We speculated that cold stress in *C. elegans* may change the enzymatic activities of rRNA processing and maturation machineries and alter rRNA production, which leads to nucleolar reshaping.

### The function of NoVs

The NoV is an evolutionarily conserved nucleolar subcompartment, but its function remains unclear. We found that a certain proportion of nucleoli in various tissues in wild-type *C. elegans* were vacuole contained with the NoV inside. In intestinal cells, approximately 90% of the nucleoli have NoVs from larva to gravid adult. Of note, the NoVs in the germline nucleoli revealed dynamic changes during aging. Previous studies have shown that NoVs appear mainly in actively transcribing nucleoli in plants.<sup>12,15,19,38</sup> It was also speculated that the size of the vacuole represents nucleolar activities in plants.<sup>15,16</sup> In addition, several studies have shown that larger nucleoli mean higher rRNA generation activities.<sup>68–70</sup> Compared with the epidermal nucleus, the intestinal nucleus, which is 32-ploid,<sup>71</sup> has a larger nucleolus, suggesting a more active rRNA transcription in intestinal nucleoli.

We speculated that the expression and processing of rRNAs are differentially regulated across different cell types and throughout development and aging, which induced the formation of cell-type-specific nucleolar structures and the change of NoVs during germline maturity and aging of the animals. Therefore, it is beneficial for understanding the function of NoV by building up new tools to directly visualize the expression and processing of rRNAs at single-cell levels.

During germline development, an mRNA transporter, NXF-1, was specifically enriched in the NoV of the germline in gravid adult worms. Furthermore, the NoV was enriched with many nucleoplasmic proteins. Despite the nucleolar ring separating the NoV from the nucleoplasm, there is a rapid component exchange between these two compartments. These data suggested that NoVs may have important roles in germline development or mRNA metabolism. Consistently, previous studies showed that NoVs may be involved in the transport of nucleolar substance from the nucleolus to the nucleoplasm and in the temporary storage of certain materials.<sup>12,13,22</sup> In tobacco BY-2 cells,

time-lapse photography revealed that the NoV slowly disappears over time.<sup>22</sup> We also observed a dynamic change of NoV over time in the oocyte nucleoli of *C. elegans*, suggesting that the vacuole is not a simple material storage place but rather plays important regulatory roles.

### Limitations of the study

Recent reports showed that nucleoli in *C. elegans* contain two canonical subcompartments: the GC and the FC.<sup>9</sup> Due to the limitation of our microscope resolution, we did not assay the change of the GC/FC subnucleolar structures in nucleoli with large NoVs upon knocking down class I RPLs. Therefore, it is unclear whether the localization of GC- and FC-associated proteins are altered in *C. elegans* under these conditions. Meanwhile, this work only focused on the regulation of NoVs in *C. elegans*; whether and how the regulation of NoVs is conserved in other species is unknown.

### STAR★METHODS

Detailed methods are provided in the online version of this paper and include the following:

- KEY RESOURCES TABLE
- RESOURCE AVAILABILITY
  - Lead contact
  - Materials availability
  - Data and code availability
- EXPERIMENTAL MODEL AND SUBJECT PARTICIPANT DETAILS
  - *C. elegans* strains
- METHOD DETAILS
  - Candidate-based RNAi screening
  - Imaging
  - Construction of plasmids and transgenic strains
  - CRISPR/Cas9-mediated gene editing
  - Actinomycin D treatment
  - Fluorescence recovery after photo bleaching (FRAP)
  - DAPI staining
  - RNA staining
  - cRT-PCR
  - Quantitative real-time PCR
- QUANTIFICATION AND STATISTICAL ANALYSIS
  - Statistics

### SUPPLEMENTAL INFORMATION

Supplemental information can be found online at <https://doi.org/10.1016/j.celrep.2023.112915>.

### ACKNOWLEDGMENTS

We are grateful to the members of the Guang laboratory for their comments and to Ruining Cai from the Institute of Oceanology, Chinese Academy of Sciences, Qingdao, China. We are grateful to the International *C. elegans* Gene Knockout Consortium and the National Bioresource Project for providing the strains. Some strains were provided by the Caenorhabditis Genetics Center (CGC), which is funded by the NIH Office of Research Infrastructure Programs (grant P40 OD010440). This work was supported by grants from the National Key R&D Program of China (2022YFA1302700 and 2019YFA0802600) and

the National Natural Science Foundation of China (32230016, 91940303, 32270583, 32070619, 31870812, 31871300, and 31900434). This study was supported in part by the Fundamental Research Funds for the Central Universities.

### AUTHOR CONTRIBUTIONS

C.Z., X.F., and S.G. designed the project; D.X., X.C., Y.K., M.H., T.X., K.W., X.H., C.F., and K.R. performed research; D.X. and X.C. contributed to RNAi screens and cRT-PCR analysis; X.C., Y.K., M.H., T.X., K.W., and X.H. contributed to transgene construction; and D.X. and S.G. wrote the paper.

### DECLARATION OF INTERESTS

The authors declare no competing interests.

Received: April 17, 2023

Revised: July 3, 2023

Accepted: July 17, 2023

### REFERENCES

1. McStay, B. (2016). Nucleolar organizer regions: genomic 'dark matter' requiring illumination. *Genes Dev.* 30, 1598–1610. <https://doi.org/10.1101/gad.283838.116>.
2. Thul, P.J., Åkesson, L., Wiking, M., Mahdessian, D., Geladaki, A., Ait Blal, H., Alm, T., Asplund, A., Björk, L., Breckels, L.M., et al. (2017). A subcellular map of the human proteome. *Science* 356, eaal3321. <https://doi.org/10.1126/science.aal3321>.
3. Stenström, L., Mahdessian, D., Gnann, C., Cesnik, A.J., Ouyang, W., Leonetti, M.D., Uhlén, M., Cuylen-Haering, S., Thul, P.J., and Lundberg, E. (2020). Mapping the nucleolar proteome reveals a spatiotemporal organization related to intrinsic protein disorder. *Mol. Syst. Biol.* 16, e9469. <https://doi.org/10.15252/msb.20209469>.
4. Feric, M., Vaidya, N., Harmon, T.S., Mitrea, D.M., Zhu, L., Richardson, T.M., Kriwacki, R.W., Pappu, R.V., and Brangwynne, C.P. (2016). Coexisting liquid phases underlie nucleolar subcompartments. *Cell* 165, 1686–1697. <https://doi.org/10.1016/j.cell.2016.04.047>.
5. Brangwynne, C.P., Mitchison, T.J., and Hyman, A.A. (2011). Active liquid-like behavior of nucleoli determines their size and shape in *Xenopus laevis* oocytes. *Proc. Natl. Acad. Sci. USA* 108, 4334–4339. <https://doi.org/10.1073/pnas.1017150108>.
6. Weber, S.C., and Brangwynne, C.P. (2015). Inverse size scaling of the nucleolus by a concentration-dependent phase transition. *Curr. Biol.* 25, 641–646. <https://doi.org/10.1016/j.cub.2015.01.012>.
7. Lafontaine, D.L.J., Riback, J.A., Bascetin, R., and Brangwynne, C.P. (2021). The nucleolus as a multiphase liquid condensate. *Nat Rev Mol Cell Biol* 22, 165–182. <https://doi.org/10.1038/s41580-020-0272-6>.
8. Kaur, T., Raju, M., Alshareedah, I., Davis, R.B., Potoyan, D.A., and Banerjee, P.R. (2021). Sequence-encoded and composition-dependent protein-RNA interactions control multiphase condensate morphologies. *Nat. Commun.* 12, 872. <https://doi.org/10.1038/s41467-021-21089-4>.
9. Spaulding, E.L., Feidler, A.M., Cook, L.A., and Updike, D.L. (2022). RG/RGG repeats in the *C. elegans* homologs of Nucleolin and GAR1 contribute to sub-nucleolar phase separation. *Nat. Commun.* 13, 6585. <https://doi.org/10.1038/s41467-022-34225-5>.
10. Shaw, P.J., and Brown, J.W.S. (2004). Plant nuclear bodies. *Curr. Opin. Plant Biol.* 7, 614–620. <https://doi.org/10.1016/j.pbi.2004.09.011>.
11. Montgomery, T.S.H. (1898). Comparative cytological studies with especial regard to the morphology of the nucleolus. *J. Morphol.* 15, 265–582. <https://doi.org/10.1002/jmor.1050150204>.

12. Johnson, J.M., and Jones, L.E. (1967). Behavior of nucleoli and contracting nucleolar vacuoles in tobacco cells growing in microculture. *Am. J. Bot.* 54, 189–198. <https://doi.org/10.2307/2440797>.
13. Rose, R.J., Setterfield, G., and Fowke, L.C. (1972). Activation of nucleoli in tuber slices and the function of nucleolar vacuoles. *Exp. Cell Res.* 71, 1–16. [https://doi.org/10.1016/0014-4827\(72\)90256-x](https://doi.org/10.1016/0014-4827(72)90256-x).
14. Krüger, T., and Scheer, U. (2010). p53 localizes to intranucleolar regions distinct from the ribosome production compartments. *J. Cell Sci.* 123, 1203–1208. <https://doi.org/10.1242/jcs.062398>.
15. Stępiński, D. (2014). Functional ultrastructure of the plant nucleolus. *Protoplasma* 251, 1285–1306. <https://doi.org/10.1007/s00709-014-0648-6>.
16. Stępiński, D. (2008). Nucleolar vacuolation in soybean root meristematic cells during recovery after chilling. *Biol. Plant. (Prague)* 52, 507–512. <https://doi.org/10.1007/s10535-008-0098-0>.
17. Hayashi, K., and Matsunaga, S. (2019). Heat and chilling stress induce nucleolus morphological changes. *J. Plant Res.* 132, 395–403. <https://doi.org/10.1007/s10265-019-01096-9>.
18. Johnson, J.M. (1969). A study of nucleolar vacuoles in cultured tobacco cells using radioautography, actinomycin d, and electron microscopy. *J. Cell Biol.* 43, 197–206. <https://doi.org/10.1083/jcb.43.2.197>.
19. Debarsy, T., Deltour, R., and Bronchart, R. (1974). Study of nucleolar vacuolation and ma-synthesis in embryonic root cells of zea-mays. *J. Cell Sci.* 16, 95–112. <https://doi.org/10.1242/jcs.16.1.95>.
20. Beven, A.F., Simpson, G.G., Brown, J.W., and Shaw, P.J. (1995). The organization of spliceosomal components in the nuclei of higher plants. *J. Cell Sci.* 108, 509–518. <https://doi.org/10.1242/jcs.108.2.509>.
21. Beven, A.F., Lee, R., Razaz, M., Leader, D.J., Brown, J.W., and Shaw, P.J. (1996). The organization of ribosomal RNA processing correlates with the distribution of nucleolar snRNAs. *J. Cell Sci.* 109, 1241–1251. <https://doi.org/10.1242/jcs.109.6.1241>.
22. Reichow, S.L., Hamma, T., Ferré-D'Amaré, A.R., and Varani, G. (2007). The structure and function of small nucleolar ribonucleoproteins. *Nucleic Acids Res.* 35, 1452–1464. <https://doi.org/10.1093/nar/gkl1172>.
23. Zhu, C., Yan, Q., Weng, C., Hou, X., Mao, H., Liu, D., Feng, X., and Guang, S. (2018). Erroneous ribosomal RNAs promote the generation of antisense ribosomal siRNA. *Proc. Natl. Acad. Sci. USA* 115, 10082–10087. <https://doi.org/10.1073/pnas.1800974115>.
24. Yokoyama, W., Hirota, K., Wan, H., Sumi, N., Miyata, M., Araoi, S., Nomura, N., Kako, K., and Fukamizu, A. (2018). rRNA adenine methylation requires T07A9.8 gene as rram-1 in *Caenorhabditis elegans*. *J. Biochem.* 163, 465–474. <https://doi.org/10.1093/jb/mvy018>.
25. Falahati, H., and Wieschhaus, E. (2017). Independent active and thermodynamic processes govern the nucleolus assembly in vivo. *Proc. Natl. Acad. Sci. USA* 114, 1335–1340. <https://doi.org/10.1073/pnas.1615395114>.
26. Yoshizawa, T., Ali, R., Jiou, J., Fung, H.Y.J., Burke, K.A., Kim, S.J., Lin, Y., Peebles, W.B., Saltzberg, D., Soniat, M., et al. (2018). nuclear import receptor inhibits phase separation of FUS through binding to multiple sites. *Cell* 173, 693–705.e22. <https://doi.org/10.1016/j.cell.2018.03.003>.
27. Ruff, K.M., Roberts, S., Chilkoti, A., and Pappu, R.V. (2018). advances in understanding stimulus responsive phase behavior of intrinsically disordered protein polymers. *J. Mol. Biol.* 430, 4619–4635. <https://doi.org/10.1016/j.jmb.2018.06.031>.
28. Zhang, G., Wang, Z., Du, Z., and Zhang, H. (2018). mTOR regulates phase separation of pgl granules to modulate their autophagic degradation. *Cell* 174, 1492–1506.e22. <https://doi.org/10.1016/j.cell.2018.08.006>.
29. Pullara, P., Alshareedah, I., and Banerjee, P.R. (2022). Temperature-dependent reentrant phase transition of RNA-polycation mixtures. *Soft Matter* 18, 1342–1349. <https://doi.org/10.1039/d1sm01557e>.
30. Wadsworth, G.M., Zahurancik, W.J., Zeng, X., Pullara, P., Lai, L.B., Sidharthan, V., Pappu, R.V., Gopalan, V., Banerjee, P.R., and Banerjee, P.R. (2022). RNAs undergo phase transitions with lower critical solution temperatures. Preprint at bioRxiv. <https://doi.org/10.1101/2022.10.17.512593>.
31. Shan, L., Xu, G., Yao, R.W., Luan, P.F., Huang, Y., Zhang, P.H., Pan, Y.H., Zhang, L., Gao, X., Li, Y., et al. (2023). Nucleolar URB1 ensures 3' ETS rRNA removal to prevent exosome surveillance. *Nature* 615, 526–534. <https://doi.org/10.1038/s41586-023-05767-5>.
32. Pham, K., Masoudi, N., Leyva-Díaz, E., and Hobert, O. (2021). A nervous system-specific subnuclear organelle in *Caenorhabditis elegans*. *Genetics* 217, 1–17. <https://doi.org/10.1093/genetics/iyaa016>.
33. Korčėková, D., Gombitová, A., Raška, I., Cmarko, D., and Lanctôt, C. (2012). Nucleologenesis in the *Caenorhabditis elegans* embryo. *PLoS One* 7, e40290. <https://doi.org/10.1371/journal.pone.0040290>.
34. Zatsėpina, O., Baly, C., Chebrou, M., and Debey, P. (2003). The step-wise assembly of a functional nucleolus in preimplantation mouse embryos involves the cajal (coiled) body. *Dev. Biol.* 253, 66–83. <https://doi.org/10.1006/dbio.2002.0865>.
35. Saijou, E., Fujiwara, T., Suzuki, T., Inoue, K., and Sakamoto, H. (2004). RBD-1, a nucleolar RNA-binding protein, is essential for *Caenorhabditis elegans* early development through 18S ribosomal RNA processing. *Nucleic Acids Res.* 32, 1028–1036. <https://doi.org/10.1093/nar/gkh264>.
36. Pendle, A.F., Clark, G.P., Boon, R., Lewandowska, D., Lam, Y.W., Andersen, J., Mann, M., Lamond, A.I., Brown, J.W.S., and Shaw, P.J. (2005). Proteomic analysis of the Arabidopsis nucleolus suggests novel nucleolar functions. *Mol. Biol. Cell* 16, 260–269. <https://doi.org/10.1091/mbc.e04-09-0791>.
37. Jordan, E.G. (1984). Nucleolar Nomenclature. *J. Cell Sci.* 67, 217–220. <https://doi.org/10.1242/jcs.67.1.217>.
38. Deltour, R., and de Barsy, T. (1985). Nucleolar activation and vacuolation in embryo radicle cells during early germination. *J. Cell Sci.* 76, 67–83. <https://doi.org/10.1242/jcs.76.1.67>.
39. Wan, G., Yan, J., Fei, Y., Pagano, D.J., and Kennedy, S. (2020). A Conserved NRDE-2/MTR-4 Complex Mediates Nuclear RNAi in *Caenorhabditis elegans*. *Genetics* 216, 1071–1085. <https://doi.org/10.1534/genetics.120.303631>.
40. Akay, A., Di Domenico, T., Suen, K.M., Nabih, A., Parada, G.E., Larence, M., Medhi, R., Berkuyrek, A.C., Zhang, X., Wedeles, C.J., et al. (2017). The helicase aquarius/EMB-4 is required to overcome intronic barriers to allow nuclear RNAi pathways to heritably silence transcription. *Dev. Cell* 42, 241–255.e6. <https://doi.org/10.1016/j.devcel.2017.07.002>.
41. Guang, S., Bochner, A.F., Pavelec, D.M., Burkhart, K.B., Harding, S., Lachowicz, J., and Kennedy, S. (2008). An argonaute transports siRNAs from the cytoplasm to the nucleus. *Science* 321, 537–541. <https://doi.org/10.1126/science.1157647>.
42. Guang, S., Bochner, A.F., Burkhart, K.B., Burton, N., Pavelec, D.M., and Kennedy, S. (2010). Small regulatory RNAs inhibit RNA polymerase II during the elongation phase of transcription. *Nature* 465, 1097–1101. <https://doi.org/10.1038/nature09095>.
43. Liao, S., Chen, X., Xu, T., Jin, Q., Xu, Z., Xu, D., Zhou, X., Zhu, C., Guang, S., and Feng, X. (2021). Antisense ribosomal siRNAs inhibit RNA polymerase I-directed transcription in *C. elegans*. *Nucleic Acids Res.* 49, 9194–9210. <https://doi.org/10.1093/nar/gkab662>.
44. Sheth, U., Pitt, J., Dennis, S., and Priess, J.R. (2010). Perinuclear P granules are the principal sites of mRNA export in adult *C. elegans* germ cells. *Development* 137, 1305–1314. <https://doi.org/10.1242/dev.044255>.
45. Gamalinda, M., Ohmayer, U., Jakovljevic, J., Kumcuoglu, B., Woolford, J., Mbom, B., Lin, L., and Woolford, J.L. (2014). A hierarchical model for assembly of eukaryotic 60S ribosomal subunit domains. *Gene Dev.* 28, 198–210. <https://doi.org/10.1101/gad.228825.113>.
46. Hang, R., Wang, Z., Deng, X., Liu, C., Yan, B., Yang, C., Song, X., Mo, B., and Cao, X. (2018). Ribosomal RNA biogenesis and its response to chilling stress in *oryza sativa*. *Plant Physiol.* 177, 381–397. <https://doi.org/10.1104/pp.17.01714>.
47. Zakrzewska-Placzek, M., Souret, F.F., Sobczyk, G.J., Green, P.J., and Kufel, J. (2010). Arabidopsis thaliana XRN2 is required for primary cleavage in

- the pre-ribosomal RNA. *Nucleic Acids Res.* 38, 4487–4502. <https://doi.org/10.1093/nar/gkq172>.
48. Gabel, H.W., and Ruvkun, G. (2008). The exonuclease ERI-1 has a conserved dual role in 5.8S rRNA processing and RNAi. *Nat. Struct. Mol. Biol.* 15, 531–533. <https://doi.org/10.1038/nsmb.1411>.
  49. Zhou, X., Feng, X., Mao, H., Li, M., Xu, F., Hu, K., and Guang, S. (2017). RdRP-synthesized antisense ribosomal siRNAs silence pre-rRNA via the nuclear RNAi pathway. *Nat. Struct. Mol. Biol.* 24, 258–269. <https://doi.org/10.1038/nsmb.3376>.
  50. Klinge, S., and Woolford, J.L., Jr. (2019). Ribosome assembly coming into focus. *Nat. Rev. Mol. Cell Biol.* 20, 116–131. <https://doi.org/10.1038/s41580-018-0078-y>.
  51. Hiraishi, N., Ishida, Y.I., Sudo, H., and Nagahama, M. (2018). WDR74 participates in an early cleavage of the pre-rRNA processing pathway in cooperation with the nucleolar AAA-ATPase NVL2. *Biochem Biophys Res Commun* 495, 116–123. <https://doi.org/10.1016/j.bbrc.2017.10.148>.
  52. Horsey, E.W., Jakovljevic, J., Miles, T.D., Hampicharnchai, P., and Woolford, J.L. (2004). Role of yeast Rrp1 protein in the dynamics of pre-ribosome maturation. *Rna* 10, 813–827. <https://doi.org/10.1261/rna.5255804>.
  53. Yang, P., Mathieu, C., Kolaitis, R.M., Zhang, P., Messing, J., Yurtsever, U., Yang, Z., Wu, J., Li, Y., Pan, Q., et al. (2020). G3BP1 is a tunable switch that triggers phase separation to assemble stress granules. *Cell* 181, 325–345.e28. <https://doi.org/10.1016/j.cell.2020.03.046>.
  54. Elbaum-Garfinkle, S., Kim, Y., Szczepaniak, K., Chen, C.C.H., Eckmann, C.R., Myong, S., and Brangwynne, C.P. (2015). The disordered P granule protein LAF-1 drives phase separation into droplets with tunable viscosity and dynamics. *Proc. Natl. Acad. Sci. USA* 112, 7189–7194. <https://doi.org/10.1073/pnas.1504822112>.
  55. Chong, P.A., Vernon, R.M., and Forman-Kay, J.D. (2018). RGG/RG Motif Regions in RNA Binding and Phase Separation. *J. Mol. Biol.* 430, 4650–4665. <https://doi.org/10.1016/j.jmb.2018.06.014>.
  56. Giniasty, H., Sicard, H., Roger, B., and Bouvet, P. (1999). Structure and functions of nucleolin. *J. Cell Sci.* 112, 761–772. <https://doi.org/10.1242/jcs.112.6.761>.
  57. Frottin, F., Schueder, F., Tiwary, S., Gupta, R., Körner, R., Schlichthaerle, T., Cox, J., Jungmann, R., Hartl, F.U., and Hipp, M.S. (2019). The nucleolus functions as a phase-separated protein quality control compartment. *Science* 365, 342–347. <https://doi.org/10.1126/science.aaw9157>.
  58. Banerjee, P.R., Milin, A.N., Moosa, M.M., Onuchic, P.L., and Deniz, A.A. (2017). Reentrant phase transition drives dynamic substructure formation in ribonucleoprotein droplets. *Angew Chem Int Edit* 56, 11354–11359. <https://doi.org/10.1002/anie.201703191>.
  59. Alshareedah, I., Kaur, T., Ngo, J., Seppala, H., Kounatse, L.A.D., Wang, W., Moosa, M.M., and Banerjee, P.R. (2019). Interplay between short-range attraction and long-range repulsion controls reentrant liquid condensation of ribonucleoprotein-RNA complexes. *J. Am. Chem. Soc.* 141, 14593–14602. <https://doi.org/10.1021/jacs.9b03689>.
  60. Alshareedah, I., Moosa, M.M., Raju, M., Potoyan, D.A., and Banerjee, P.R. (2020). Phase transition of RNA-protein complexes into ordered hollow condensates. *Proc. Natl. Acad. Sci. USA* 117, 15650–15658. <https://doi.org/10.1073/pnas.1922365117>.
  61. Shav-Tal, Y., Blechman, J., Darzacq, X., Montagna, C., Dye, B.T., Patton, J.G., Singer, R.H., and Zipori, D. (2005). Dynamic sorting of nuclear components into distinct nucleolar caps during transcriptional inhibition. *Mol. Biol. Cell* 16, 2395–2413. <https://doi.org/10.1091/mbc.e04-11-0992>.
  62. Yin, Y., Niu, L., Zhu, X., Zhao, M., Zhang, Z., Mann, S., and Liang, D. (2016). Non-equilibrium behaviour in coacervate-based protocells under electric-field-induced excitation. *Nat. Commun.* 7, 10658. <https://doi.org/10.1038/ncomms10658>.
  63. Yu, H., Lu, S., Gasior, K., Singh, D., Vazquez-Sanchez, S., Tapia, O., Toprani, D., Beccari, M.S., Yates, J.R., 3rd, Da Cruz, S., et al. (2021). HSP70 chaperones RNA-free TDP-43 into anisotropic intranuclear liquid spherical shells. *Science* 371, eabb4309. <https://doi.org/10.1126/science.abb4309>.
  64. Ries, R.J., Zaccara, S., Klein, P., Olarerin-George, A., Namkoong, S., Pickering, B.F., Patil, D.P., Kwak, H., Lee, J.H., and Jaffrey, S.R. (2019). m(6)A enhances the phase separation potential of mRNA. *Nature* 571, 424–428. <https://doi.org/10.1038/s41586-019-1374-1>.
  65. Henninger, J.E., Oksuz, O., Shrinivas, K., Sagi, I., LeRoy, G., Zheng, M.M., Andrews, J.O., Zamudio, A.V., Lazaris, C., Hannett, N.M., et al. (2021). RNA-mediated feedback control of transcriptional condensates. *Cell* 184, 207–225.e24. <https://doi.org/10.1016/j.cell.2020.11.030>.
  66. Boulon, S., Westman, B.J., Hutten, S., Boisvert, F.M., and Lamond, A.I. (2010). The nucleolus under stress. *Mol. Cell* 40, 216–227. <https://doi.org/10.1016/j.molcel.2010.09.024>.
  67. Szaflarski, W., Leśniczak-Staszak, M., Sowiński, M., Ojha, S., Aulas, A., Dave, D., Malla, S., Anderson, P., Ivanov, P., and Lyons, S.M. (2022). Early rRNA processing is a stress-dependent regulatory event whose inhibition maintains nucleolar integrity. *Nucleic Acids Res.* 50, 1033–1051. <https://doi.org/10.1093/nar/gkab1231>.
  68. Frank, D.J., and Roth, M.B. (1998). ncl-1 is required for the regulation of cell size and ribosomal RNA synthesis in *Caenorhabditis elegans*. *J. Cell Biol.* 140, 1321–1329. <https://doi.org/10.1083/jcb.140.6.1321>.
  69. Neumüller, R.A., Gross, T., Samsonova, A.A., Vinayagam, A., Buckner, M., Founk, K., Hu, Y., Sharifpoor, S., Rosebrock, A.P., Andrews, B., et al. (2013). conserved regulators of nucleolar size revealed by global phenotypic analyses. *Sci. Signal.* 6, ra70. <https://doi.org/10.1126/scisignal.2004145>.
  70. Tiku, V., Jain, C., Raz, Y., Nakamura, S., Heestand, B., Liu, W., Späth, M., Suchiman, H.E.D., Müller, R.U., Slagboom, P.E., et al. (2017). Small nucleoli are a cellular hallmark of longevity. *Nat. Commun.* 8, 16083. <https://doi.org/10.1038/ncomms16083>.
  71. Hedgecock, E.M., and White, J.G. (1985). polyploid tissues in the nematode *Caenorhabditis elegans*. *Dev. Biol.* 107, 128–133. [https://doi.org/10.1016/0012-1606\(85\)90381-1](https://doi.org/10.1016/0012-1606(85)90381-1).
  72. Timmons, L., Court, D.L., and Fire, A. (2001). Ingestion of bacterially expressed dsRNAs can produce specific and potent genetic interference in *Caenorhabditis elegans*. *Gene* 263, 103–112. [https://doi.org/10.1016/s0378-1119\(00\)00579-5](https://doi.org/10.1016/s0378-1119(00)00579-5).
  73. Kamath, R.S., Fraser, A.G., Dong, Y., Poulin, G., Durbin, R., Gotta, M., Kanapin, A., Le Bot, N., Moreno, S., Sohrmann, M., et al. (2003). Systematic functional analysis of the *Caenorhabditis elegans* genome using RNAi. *Nature* 421, 231–237. <https://doi.org/10.1038/nature01278>.

## STAR★METHODS

### KEY RESOURCES TABLE

REAGENT or RESOURCE	SOURCE	IDENTIFIER
<b>Critical commercial assays</b>		
GoScript Reverse Transcription System	Promega	Cat#A5000/A50001
SYBR Green	Vazyme	Cat#Q111-02/03
ClonExpress MultiS One Step Cloning Kit	Vazyme	Cat#C113-02
T4 RNA ligase I (ssRNA Ligase)	BioLabs	Cat#M0204SVIAL
Actinomycin D	MCE	Cat#HY-17559
SYTO RNASelect Green	Invitrogen	Cat#S32703
<b>Experimental models: Organisms/strains</b>		
<i>C. elegans</i> Strains, see <a href="#">Table S2</a>	This Paper	N/A
<b>Oligonucleotides</b>		
Sequences of double-strand RNA for RNAi, see <a href="#">Table S3</a>	This Paper	N/A
Primers for ectopic transgenes construction, see <a href="#">Table S4</a>	This Paper	N/A
Primers for <i>in situ</i> transgenes construction, see <a href="#">Table S5</a>	This Paper	N/A
Sequences for sgRNA-mediated gene editing, see <a href="#">Table S6</a>	This Paper	N/A
Primers for cRT and qRT assays, see <a href="#">Table S7</a>	This Paper	N/A
<b>Other</b>		
Selected rRNA processing and ribosome assembly factors tested by RNAi screening, see <a href="#">Table S1</a>	This Paper	N/A

### RESOURCE AVAILABILITY

#### Lead contact

Further information and requests for resources and reagents should be directed to and will be fulfilled by the lead contact, Shouhong Guang ([sguang@ustc.edu.cn](mailto:sguang@ustc.edu.cn)).

#### Materials availability

This study did not generate new unique reagents.

#### Data and code availability

All data reported in this paper will be shared by the [lead contact](#) upon request. This paper does not report original code. Any additional information required to reanalyze the data reported in this paper is available from the [lead contact](#) upon request.

### EXPERIMENTAL MODEL AND SUBJECT PARTICIPANT DETAILS

#### *C. elegans* strains

Bristol strain N2 was used as the standard wild-type strain. All strains were grown at 20°C unless otherwise specified. The strains used in this study are listed in [Table S2](#).

### METHOD DETAILS

#### Candidate-based RNAi screening

RNAi experiments were performed at 20°C by placing synchronized embryos on feeding RNAi plates as previously described.<sup>72</sup> HT115 bacteria expressing the empty vector L4440 (a gift from A. Fire) were used as controls. Bacterial clones expressing double-stranded RNAs (dsRNAs) were obtained from the Ahringer RNAi library<sup>73</sup> and sequenced to verify their identity. Some bacterial clones were constructed in this work, which are listed in [Table S3](#). All RNAi feeding experiments were performed for two generations except for larval arrest or sterile worms.

### Imaging

Images were collected using a Leica DM4B microscope. All worms were imaged at L3-L4 stage unless otherwise specified.

### Construction of plasmids and transgenic strains

For ectopic transgenes, the promoter and CDS region and UTR were amplified from N2 genomic DNA. The mCherry coding sequence was amplified from PFCJ90. The vector fragment was PCR amplified from plasmid pSG274. These fragments were joined together by Gibson assembly to form the repair plasmid with the ClonExpress MultiS One Step Cloning Kit (Vazyme Biotech, Nanjing, China, Cat. No. C113-01/02). The transgene was integrated into *C. elegans* chromosome II via a modified counterselection (cs)-CRISPR method. The sequences of the primers are listed in [Table S4](#).

For *in situ* knock-in transgenes, the 3xFLAG::GFP coding region was PCR amplified from shg1248 genomic DNA. The GFP:3xFLAG coding region was PCR amplified from shg2123 genomic DNA. The mCherry coding region was PCR amplified from shg1660 genomic DNA. The tagRFP coding region was PCR amplified from YY1446 genomic DNA. Homologous left and right arms (1.5 kb) were PCR amplified from N2 genomic DNA. The backbone was PCR amplified from the plasmid pCFJ151. All these fragments were joined together by Gibson assembly to form the repair plasmid with the ClonExpress MultiS One Step Cloning Kit (Vazyme Biotech, Nanjing, China, Cat. No. C113-01/02). This plasmid was coinjected into N2 animals with three sgRNA expression vectors, 5 ng/ $\mu$ L pCFJ90 and the Cas9 II-expressing plasmid. The sequences of the primers are listed in [Table S5](#).

### CRISPR/Cas9-mediated gene editing

For the *nucl-1(ust313)* in-frame mutant, a 1.5 kb homologous left arm was PCR amplified with the primers 5'-GGGTAACGCCAG CACGTGTGGCCAAAGTTTAATCACCTCGCTCGC-3' and 5'-TCGCTAAAACCAACTCGGCTTGAGTCGAAACCCATTTTGATTG TACC-3'. A 1 kb homologous right arm was PCR amplified with the primers 5'-AGCCGAGTTGGTTTTAGCGATAAGAGAA AACAGTATGATAG-3' and 5'-CAGCGGATAACAATTTACATCATCTTCATCCTCATCGTC-3'. The backbone was PCR amplified from the plasmid pCFJ151 with the primers 5'-CACACGTGCTGGCGTTACCC-3' and 5'-TGTGAAATTGTTATCCGCTGG-3'. All these fragments were joined together by Gibson assembly to form the *nucl-1* plasmid with the ClonExpress MultiS One Step Cloning Kit (Vazyme Biotech, Nanjing, China, Cat. No. C113-01/02). This plasmid was coinjected into N2 animals with three sgRNA expression vectors, *nucl-1* sgRNA#1/#2/#3, 5 ng/ $\mu$ L pCFJ90 and Cas9 II expressing plasmid.

The sgRNAs used in this study for transgene construction are listed in [Table S6](#).

### Actinomycin D treatment

Actinomycin D (MedChemExpress no. HY-17559, CAS:50-76-0) was prepared at 20 mg/mL in DMSO as a stock solution. Each 3.5  $\mu$ L actinomycin D stock solution was diluted with 300  $\mu$ L Luria-Bertani liquid medium and layered onto NGM and RNAi plates. NGM and RNAi plates were prepared and placed at 37°C overnight before use. Synchronized L1 worms were placed onto the seeded plates and grown for 48 h before imaging and collection for cRT-PCR.

### Fluorescence recovery after photo bleaching (FRAP)

FRAP experiments were performed using a Zeiss LSM980 laser scanning confocal microscope at room temperature. Worms were anesthetized with 2 mM levamisole. A region of interest was bleached with 100% laser power for 3–4 s, and the fluorescence intensities in these regions were collected every 5 s and normalized to the initial intensity before bleaching. For analysis, image intensity was measured by Mean and further analyzed by Origin software.

### DAPI staining

DNA was stained with DAPI Staining Solution (10  $\mu$ g/mL) (Biosharp, BL105A) at room temperature. Worms were fixed with 1% formaldehyde before staining and soaked in DAPI solution for 3–5 min. After washing with phosphate-buffered saline (PBS) 2–3 times, worms were imaged under a fluorescence microscope.

### RNA staining

RNA was stained with SYTO RNASelect Green Fluorescent Cell Stain (SYTO RNASelect Green Fluorescent Cell Stain-5 mM Solution in DMSO, S32703, Thermo). Worms were fixed in prechilled methanol at –20°C for 10 min before staining and then washed twice for 5 min each in PBS. The labeling solution consisted of 500 nM RNA Select Green fluorescent cell stain in phosphate-buffered saline (PBS). Worms were soaked in the 500 nM labeling solution for 20 min at room temperature, washed twice in PBS for 5 min each, and then imaged.

### cRT-PCR

Total RNA was isolated from L3 stage worms using a Dounce homogenizer (pestle B) in TRIzol solution (Invitrogen). Two micrograms of total RNA was circularized by a T4 RNA Ligase 1 Kit (M0204, NEB) and then purified by TRIzol reagent followed by isopropanol precipitation. The circularized RNA was reverse transcribed via the GoScript Reverse Transcription System (Promega #A5001). PCR was performed using 2  $\times$  Rapid Taq Master Mix (Vazyme, P222-01) for 25 cycles. The primer sets used in this work are listed in [Table S7](#).

### Quantitative real-time PCR

All quantitative real-time PCR (qPCR) experiments were performed using a MyIQ2 machine (Bio-Rad). DNA or cDNA was quantified with SYBR Green Master Mix (Vazyme, Q111-02), and qPCR was performed according to the vendor's instructions. RNA was first circularized by a T4 RNA Ligase 1 Kit (M0204, NEB) and then purified by TRIzol reagent followed by isopropanol precipitation, and then reverse transcribed via GoScript Reverse Transcription System (Promega #A5001) with indicated primers. The primer sets used in this work are listed in [Table S7](#).

### QUANTIFICATION AND STATISTICAL ANALYSIS

#### Statistics

Boxplots are presented with median and minimum and maximum. Bar graphs with error bars represented the mean and SD. All of the experiments were conducted with independent *C. elegans* animals for the indicated N times. Statistical analysis was performed with the two-tailed Student's t test. Student's t test p value threshold was set to 0.05.